LETTER

doi:10.1038/nature18641

# A combined transmission spectrum of the Earth-sized exoplanets TRAPPIST-1 b and c

Julien de Wit[1], Hannah R. Wakeford[2], Michaël Gillon[3], Nikole K. Lewis[4], Jeff A. Valenti[4], Brice-Olivier Demory[5], Adam J. Burgasser[6], Artem Burdanov[3], Laetitia Delrez[3], Emmanuël Jehin[3], Susan M. Lederer[7], Didier Queloz[5], Amaury H. M. J. Triaud[8] & Valérie Van Grootel[3]

**Three Earth-sized exoplanets were recently discovered close to the habitable zone[1,2] of the nearby ultracool dwarf star TRAPPIST-1 (ref. 3). The nature of these planets has yet to be determined, as their masses remain unmeasured and no observational constraint is available for the planetary population surrounding ultracool dwarfs, of which the TRAPPIST-1 planets are the first transiting example. Theoretical predictions span the entire atmospheric range, from depleted to extended hydrogen-dominated atmospheres[4–8]. Here we report observations of the combined transmission spectrum of the two inner planets during their simultaneous transits on 4 May 2016. The lack of features in the combined spectrum rules out cloud-free hydrogen-dominated atmospheres for each planet at $\geq 10\sigma$ levels; TRAPPIST-1 b and c are therefore unlikely to have an extended gas envelope as they occupy a region of parameter space in which high-altitude cloud/haze formation is not expected to be significant for hydrogen-dominated atmospheres[9]. Many denser atmospheres remain consistent with the featureless transmission spectrum—from a cloud-free water-vapour atmosphere to a Venus-like one.**

On 4 May 2016, we observed the simultaneous transits of the Earth-sized planets TRAPPIST-1b and TRAPPIST-1c with the Hubble Space Telescope (HST). This rare event was phased with HST's visibility window of the TRAPPIST-1 system, allowing for complete monitoring of the event (Fig. 1). Observations were conducted in 'round-trip' spatial scanning mode[10] using the near-infrared (1.1–1.7 μm) G141 grism on the wide-field camera 3 (WFC3) instrument (see Methods). Following standard practice, we monitored the transit event through four HST orbits, taking observations before, during and after the transit event to acquire accurate stellar baseline flux levels. We discarded the first orbit owing to differing systematics caused by the thermal settling of the telescope following target acquisition[11–13]. The raw light curve presents primarily ramp-like systematics on the scale of HST orbit-induced instrumental settling, discussed in previous WFC3 transit studies[11,12,14] (Fig. 1). We reduced, corrected for instrumental systematics, and analysed the data using independent methods (see Methods) that yielded consistent results. We reached an average standard deviation of normalized residuals (SDNR) of 650 parts per million (p.p.m.) per 112-second exposure (Fig. 2) on the spectrophotometric time series split in 11 channels (resolution $= \lambda/\Delta\lambda \approx 35$). Summing over the entire WFC3 spectral range, we derived a 'white' light curve with a 240-p.p.m. SDNR (Fig. 1).

We first analysed the fitting of the white-light curve for the transits of TRAPPIST-1b and TRAPPIST-1c simultaneously, while accounting for instrumental systematics. Owing to the limited phase coverage of HST observations, we fixed the system's parameters to the values provided in the discovery report[3] while estimating the transit times and depths. However, we let the band-integrated limb-darkening coefficients (LDCs) and the orbital inclinations for planets b and c ($i_b$ and $i_c$, respectively) float under the control of priors, to propagate their uncertainties on the transit depth and time estimates with which they may be correlated. These priors were derived from the PHOENIX model intensity spectra[15] for the LDCs (see Methods) and from the discovery report[3] for the planets' orbital inclinations. We find that TRAPPIST-1c

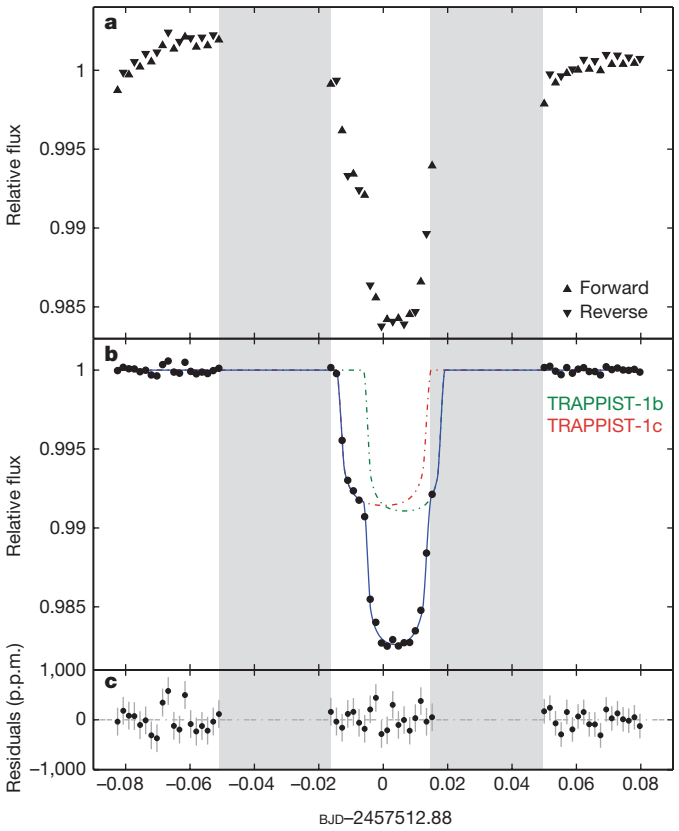


**Figure 1 | Hubble/WFC3 white-light curve for the TRAPPIST-1b and TRAPPIST-1c double transit of 4 May 2016. a**, Raw normalized white-light curve (triangles), highlighting the primary instrumental systematics (the forward/reverse flux offset and the ramp; see Methods). The shaded areas represent time windows during which no exposure was taken owing to occultation by the Earth. **b**, Normalized and systematics-corrected white-light curve (black points) and best-fit transit model (blue line). The individual contributions of TRAPPIST-1b and TRAPPIST-1c are shown in green and red, respectively. **c**, Best-fit residuals with their $1\sigma$ error bars (SDNR = 240 p.p.m.).

[1]Department of Earth, Atmospheric and Planetary Sciences, Massachusetts Institute of Technology, 77 Massachusetts Avenue, Cambridge, Massachusetts 02139, USA. [2]NASA Goddard Space Flight Center, Greenbelt, Maryland 20771, USA. [3]Institut d'Astrophysique et de Géophysique, Université de Liège, Allée du 6 Août 19C, 4000 Liège, Belgium. [4]Space Telescope Science Institute, 3700 San Martin Drive, Baltimore, Maryland 21218, USA. [5]Astrophysics Group, Cavendish Laboratory, 19 J J Thomson Avenue, Cambridge CB3 0HE, UK. [6]Center for Astrophysics and Space Science, University of California San Diego, La Jolla, California 92093, USA. [7]NASA Johnson Space Center, 2101 NASA Parkway, Houston, Texas 77058, USA. [8]Institute of Astronomy, Madingley Road, Cambridge CB3 0HA, UK.

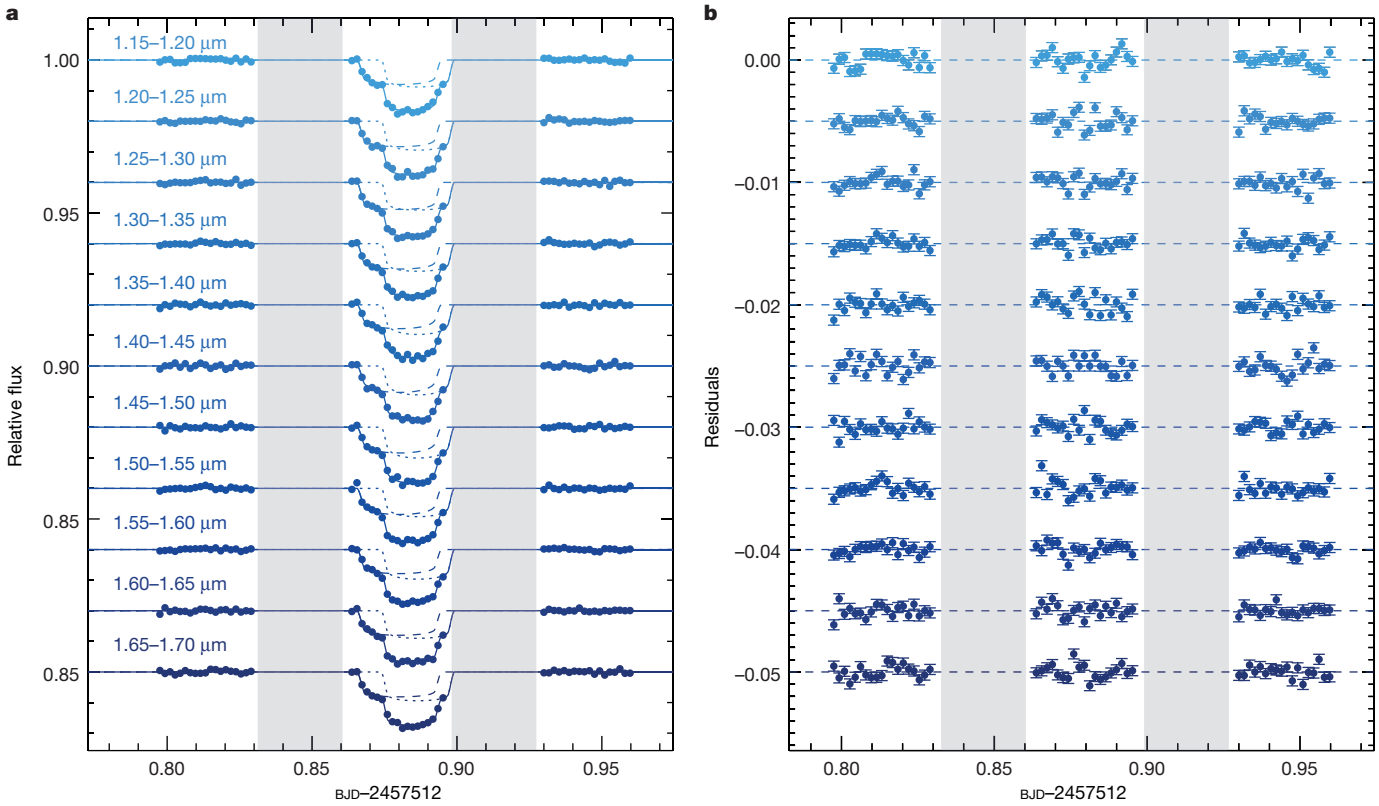


**Figure 2 | Hubble/WFC3 spectrophotometry of the TRAPPIST-1b and TRAPPIST-1c double transit of 4 May 2016. a**, Normalized and systematics-corrected data (points) and best-fit transit model (solid line) in 11 spectroscopic channels spread across the WFC3 band, offset for clarity. The individual contributions of TRAPPIST-1b and TRAPPIST-1c are shown with dotted and dashed lines, respectively. **b**, Best-fit residuals with their $1\sigma$ error bars (channel-averaged SDNR = 650 p.p.m.).

began its transit 12 minutes before TRAPPIST-1b (transit time centres at barycentric Julian date (BJD)/barycentric coordinate time (TBD) −2457512: $T_{0,b} = 0.88646 \pm 0.00030$ and $T_{0,c} = 0.88019 \pm 0.00016$; transit durations[3]: $W_b = 36.12 \pm 0.46$ min and $W_c = 41.78 \pm 0.81$ min). The difference between the planets' transit duration of $5.6 \pm 0.9$ min implies that no planet–planet eclipse[16] occurred during the observed event, given the well established orbital periods. Standard transit models[17] are therefore adequate for analysing this data set. We find an orbital inclination and transit depth across the full WFC3 band of $i_b = 89.39° \pm 0.32°$ and $\Delta F_b = 8{,}015 \pm 220$ p.p.m. for TRAPPIST-1b, and $i_c = 89.58° \pm 0.11°$ and $\Delta F_c = 7{,}290 \pm 240$ p.p.m. for TRAPPIST-1c.

In the context of double-transit observations, the data primarily constrain the combined transit depths ($\Delta F_{b+c} = 15{,}320 \pm 160$ p.p.m.). Therefore, although the partial transit of TRAPPIST-1c—before TRAPPIST-1b begins its transit—yields some constraints on $\Delta F_c$, it is not sufficient to completely lift the degeneracy between $\Delta F_b$ (being $\Delta F_{b+c} - \Delta F_c$) and $\Delta F_c$. This explains the ~30% better precision obtained with the combined transit depth, and hence also with the combined transmission spectrum. The transit depths derived over WFC3's band are in agreement, within $2\sigma$, with the values reported at discovery[3].

We then analysed the light curves in 11 spectroscopic channels, fitting for wavelength-dependent transit depths, instrumental systematics, and stellar baseline levels (Fig. 2). We tried both quadratic and four-parameter limb-darkening relationships[18] for each spectroscopic channel, because transit depth estimates may depend on the functional form used to describe limb darkening. We found, however, that our conclusions are not sensitive to which limb-darkening relationship was chosen, as long as the wavelength dependence of the LCDs is taken into account. The resulting transmission spectra are consistent with a flat line (Fig. 3).

Figure 3 shows the transit depth variations expected over the WFC3 band if TRAPPIST-1b and/or TRAPPIST-1c were harbouring a cloud-free hydrogen-dominated atmosphere (red lines and circles in Fig. 3). Our transmission spectrum model[19] sets atmospheric temperature to the planet's equilibrium temperature ($T_{eq,b} = 366$ K and $T_{eq,c} = 315$ K), assuming a Bond albedo of 0.3. Because the planetary masses remain unmeasured, we conservatively use a mass of $0.95M_\oplus$ and $0.85M_\oplus$ for TRAPPIST-1b and TRAPPIST-1c respectively ($M_\oplus$ being the mass of Earth); these are the maximum masses that allow them to possess hydrogen/helium envelopes greater than 0.1% of their total masses given their radii[20]. The precision achieved with the combined transmission spectrum (~350 p.p.m. per bin) is sufficient to detect the presence of a cloud-free hydrogen-dominated atmosphere via the detection of water or methane absorption features. The featureless spectra rule out a cloud-free, hydrogen-dominated atmosphere for TRAPPIST-1b and TRAPPIST-1c at the $12\sigma$ and $10\sigma$ level, respectively.

We also show in Fig. 3 alternative atmospheres for TRAPPIST-1b and TRAPPIST-1c that are consistent with the data; volatile (water)-rich atmospheres and hydrogen-dominated atmospheres with a cloud deck at 10 mbar are shown in blue and in yellow, respectively. Many alternatives for the atmospheres of TRAPPIST-1b and TRAPPIST-1c still remain. The atmospheric screening of sub-Neptune-sized exoplanets using existing observatories is a step-by-step process[14,21,22]. As for the super-Earth-sized planet GJ 1214b (ref. 21), the first observations of TRAPPIST-1's planets with HST allow us to rule out a cloud-free hydrogen-dominated atmosphere for either planet. If the planets' atmospheres are hydrogen-dominated, then they must contain clouds or hazes that are grey absorbers between 1.1 μm and 1.7 μm at pressures less than around 10 mbar. However, theoretical investigations for hydrogen-dominated atmospheres[9] predict that the efficiencies of haze and cloud formation at the irradiation levels of TRAPPIST-1b and TRAPPIST-1c should be dramatically reduced compared with, for example, the efficiencies for GJ 1214b (insolation ratios: $S_{GJ1214b}/S_b \approx 4$; $S_{GJ1214b}/S_c \approx 8$), leading to cloud formation at

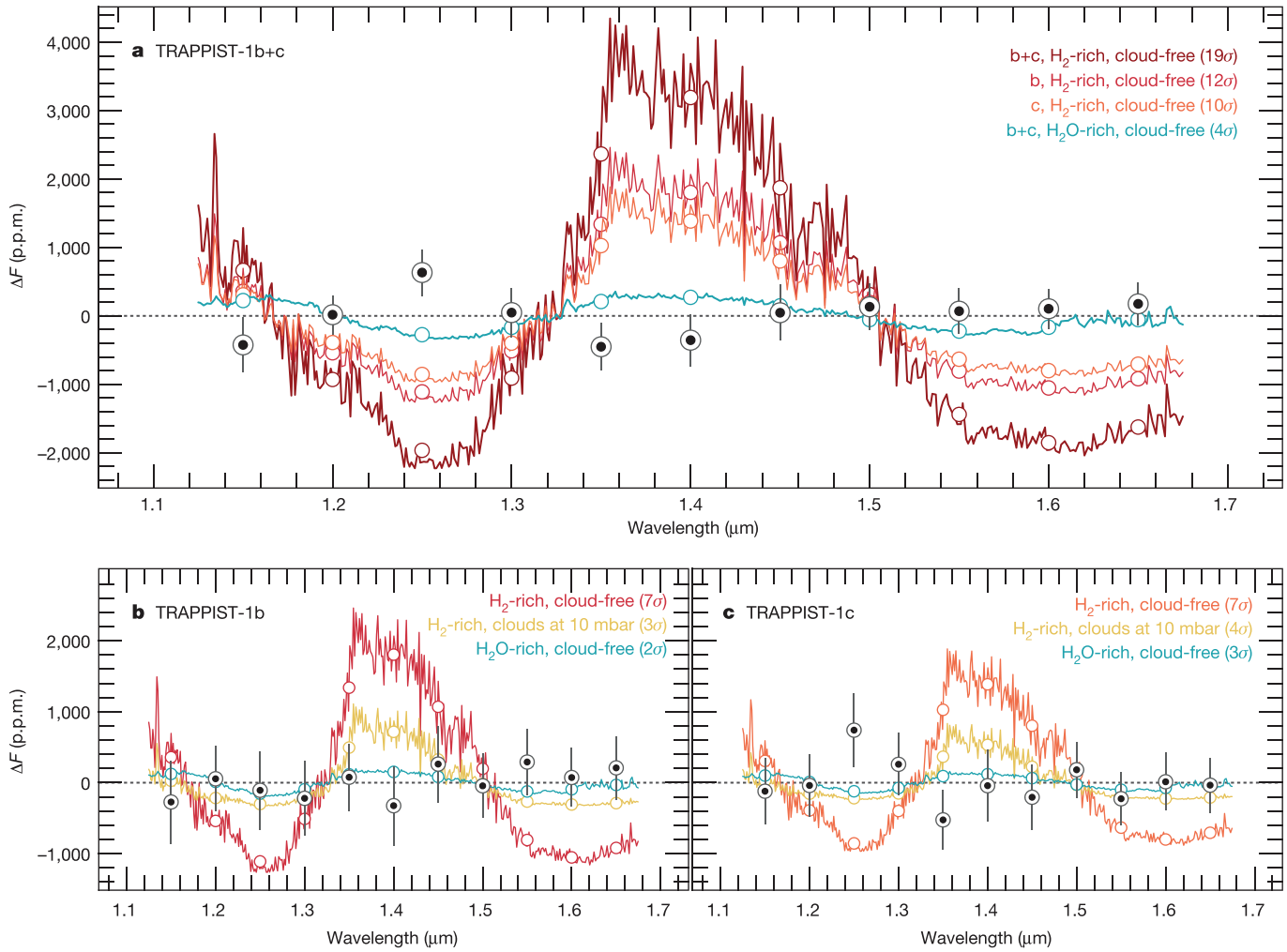


**Figure 3 | Transmission spectra of TRAPPIST-1b and TRAPPIST-1c compared with models. a–c**, Theoretical predictions of TRAPPIST-1b's transmission spectrum (**b**), TRAPPIST-1c's spectrum (**c**), and their combinations (**a**) are shown for cloud-free $H_2$-dominated atmospheres (red lines and circles), $H_2$-dominated atmospheres with a cloud deck at 10 mbar (yellow lines and circles), and cloud-free $H_2O$-dominated atmospheres (blue lines and circles). The coloured circles show the binned theoretical models. The feature at 1.4 μm arises from water absorption. The significance of the deviation of each transmission spectrum from the WFC3 measurements (black circles with 1$\sigma$ error bars) is listed in parentheses in each panel.

pressure levels of 100 mbar or more, with marginal effects on their transmission spectra[19]. In short, hydrogen-dominated atmospheres can be considered as unlikely for TRAPPIST-1b and TRAPPIST-1c.

Planets with the sizes and equilibrium temperatures of TRAPPIST-1b and TRAPPIST-1c could possess relatively thick $H_2O$-, $CO_2$-, $N_2$- or $O_2$-dominated atmospheres, or potentially tenuous atmospheres composed of a variety of chemical species[4–8,23]. All of these denser atmospheres are consistent with our measurements. The amplitude of a planet's transmission spectrum scales directly with its atmospheric mean molecular weight, $\mu$. The amplitude of an exoplanet's transmission spectrum can be expressed as $2R_p h_{eff}/R_*^2$, where $R_p$ and $R_*$ are the planetary and stellar radii, and $h_{eff}$ is the effective atmospheric height (that is, the extent of the atmospheric annulus), which is directly proportional to the atmospheric scale height, $H = kT/\mu g$, where k is Boltzmann's constant, $T$ is the atmospheric temperature, and $g$ is the surface gravity. Therefore, everything else being equal, the transmission spectrum amplitude of a denser atmosphere is significantly damped compared with the one of a hydrogen-dominated atmosphere (for example, by a factor of about seven for a $H_2O$-dominated atmosphere). As a result, no constraint on the presence and minimum pressure level of clouds/hazes for such denser atmospheres can be inferred from our data. TRAPPIST-1b and TRAPPIST-1c could, for instance, harbour a cloud-free water-vapour atmosphere or a Venus-like atmosphere with high-altitude hazes[24,25]. We shall be able soon to distinguish between such atmospheres. The transmission spectrum of Venus as an exoplanet would present broad variations of about 2 p.p.m. from 0.2 μm to 5 μm (ref. 26), which, rescaled to the TRAPPIST-1 star, correspond to variations of about 160 p.p.m. ($2 \times R_{Sun}^2/R_{TRAPPIST-1}^2$)—currently below our errors, but eventually reachable.

Screening TRAPPIST-1's Earth-sized planets now—to distinguish progressively between their plausible atmospheric regimes, and to determine their amenability for detailed atmospheric studies—will allow the optimization of follow-up studies with the next generation of observatories. Our work highlights HST/WFC3's ability to perform the first step towards a thorough understanding of these planets' atmospheric properties.

**Online Content** Methods, along with any additional Extended Data display items and Source Data, are available in the online version of the paper; references unique to these sections appear only in the online paper.

**Received 18 May; accepted 4 June 2016.**
**Published online 20 July 2016.**

1. Kopparapu, R. K. *et al.* Habitable zones around main-sequence stars: new estimates. *Astrophys. J.* **765,** 131 (2013).
2. Zsom, A., Seager, S., de Wit, J. & Stamenkovic, V. Towards the minimum inner edge distance of the habitable zone. *Astrophys. J.* **778,** 109 (2013).

3. Gillon, M. *et al.* Temperate Earth-sized planets transiting a nearby ultracool dwarf star. *Nature* **533,** 221–224 (2016).
4. Owen, J. E. & Wu, Y. Kepler planets: a tale of evaporation. *Astrophys. J.* **775,** 105 (2013).
5. Jin, S. *et al.* Planetary population synthesis coupled with atmospheric escape: a statistical view of evaporation. *Astrophys. J.* **795,** 65 (2014).
6. Johnstone, C. P. *et al.* The evolution of stellar rotation and the hydrogen atmospheres of habitable-zone terrestrial planets. *Astrophys. J.* **815,** L12 (2015).
7. Luger, R. & Barnes, R. Extreme water loss and abiotic $O_2$ buildup on planets throughout the habitable zones of M dwarfs. *Astrobiology* **15,** 119–143 (2015).
8. Owen, J. E. & Mohanty, S. Habitability of terrestrial-mass planets in the HZ of M dwarfs. I. H/He-dominated atmospheres. *Mon. Not. R. Astron. Soc.* **459,** 4088–4108 (2016).
9. Morley, C. V. *et al.* Thermal emission and reflected light spectra of super Earths with flat transmission spectra. *Astrophys. J.* **815,** 110 (2015).
10. McCullough, P. & MacKenty, J. *Considerations for using spatial scans with WFC3.* Instr. Sci. Report WFC3 2012-08 (Space Telescope Science Institute, 2012).
11. Deming, D. *et al.* Infrared transmission Spectroscopy of the exoplanets HD 209458b and XO-1b using the wide field camera-3 on the Hubble Space Telescope. *Astrophys. J.* **774,** 95 (2013).
12. Wakeford, H. R., Sing, D. K., Evans, T., Deming, D. & Mandell, A. Marginalizing instrument systematics in HST WFC3 transit light curves. *Astrophys. J.* **819,** 10 (2016).
13. Sing, D. K. *et al.* A continuum from clear to cloudy hot-Jupiter exoplanets without primordial water depletion. *Nature* **529,** 59–62 (2016).
14. Kreidberg, L. *et al.* Clouds in the atmosphere of the super-Earth exoplanet GJ1214b. *Nature* **505,** 69–72 (2014).
15. Husser, T.-O. *et al.* A new extensive library of PHOENIX stellar atmospheres and synthetic spectra. *Astron. Astrophys.* **553,** A6 (2013).
16. Hirano, T. *et al.* Planet-planet eclipse and the Rossiter-McLaughlin effect of a multiple transiting system: joint analysis of the Subaru spectroscopy and the Kepler photometry. *Astrophys. J.* **759,** L36 (2012).
17. Mandel, K. & Agol, E. Analytic light curves for planetary transit searches. *Astrophys. J.* **580,** L171–L175 (2002).
18. Sing, D. K. Stellar limb-darkening coefficients for CoRot and Kepler. *Astron. Astrophys.* **510,** A21 (2010).
19. de Wit, J. & Seager, S. Constraining exoplanet mass from transmission spectroscopy. *Science* **342,** 1473–1477 (2013).
20. Howe, A. R., Burrows, A. & Verne, W. Mass-radius relations and core-envelope decompositions of super-Earths and sub-Neptunes. *Astrophys. J.* **787,** 173 (2014).
21. Bean, J. L., Miller-Ricci Kempton, E. & Homeier, D. A ground-based transmission spectrum of the super-Earth exoplanet GJ 1214b. *Nature* **468,** 669–672 (2010).
22. Berta, Z. K. *et al.* The flat transmission spectrum of the super-Earth GJ1214b from wide field camera 3 on the Hubble Space Telescope. *Astrophys. J.* **747,** 35 (2012).
23. Leconte, J., Forget, F. & Lammer, H. On the (anticipated) diversity of terrestrial planet atmospheres. *Exp. Astron.* **40,** 449–467 (2015).
24. Tellmann, S., Pätzold, M., Häusler, B., Bird, M. K. & Tyler, G. L. Structure of the Venus neutral atmosphere as observed by the Radio Science experiment VeRa on Venus Express. *J. Geophys. Res. Planets* **114,** E00B36 (2009).
25. Wilquet, V. *et al.* Preliminary characterization of the upper haze by SPICAV/SOIR solar occultation in UV to mid-IR onboard Venus Express. *J. Geophys. Res. Planets* **114,** E00B42 (2009).
26. Ehrenreich, D. *et al.* Transmission spectrum of Venus as a transiting exoplanet. *Astron. Astrophys.* **537,** L2 (2012).


**Acknowledgements** This work is based on observations made with the NASA/ESA Hubble Space Telescope that were obtained at the Space Telescope Science Institute, which is operated by the Association of Universities for Research in Astronomy, Inc. These observations are associated with program HST-GO-14500 (principal investigator J.d.W.), support for which was provided by NASA through a grant from the Space Telescope Science Institute. The research leading to our results was funded in part by the European Research Council (ERC) under the FP/2007-2013 ERC grant 336480, and through an Action de Recherche Concertée (ARC) grant financed by the Wallonia-Brussels Federation. H.R.W. acknowledges support through an appointment to the NASA Postdoctoral Program at Goddard Space Flight Center, administered by the Universities Space Research Association through a contract with NASA. M.G. is Research Associate at the Belgian Fonds (National) de la Recherche Scientifique (FRS–FNRS). L.D. acknowledges support of the Fund for Research Training in Industry and Agriculture of the FRS–FNRS. We thank D. Taylor, S. Deustua, P. McCullough, and N. Reid for their assistance in planning and executing our observations. We are also grateful for discussions with Z. Berta-Thompson and Pierre Magain about this study and manuscript. We thank the ATLAS and PHOENIX teams for providing stellar models.

**Author Contributions** J.d.W. and H.R.W. led the data reduction and analysis, with the support of M.G., N.K.L. and B.-O.D. J.d.W., H.R.W., and N.K.L. led the data interpretation, with the support of M.G. and J.A.V. J.A.V. provided the limb-darkening coefficients and further insights into TRAPPIST-1's properties and emission together with A.J.B. Every author contributed to writing both the manuscript and the HST proposal behind these observations.

**Author Information** Reprints and permissions information is available at www.nature.com/reprints. The authors declare no competing financial interests. Readers are welcome to comment on the online version of the paper. Correspondence and requests for materials should be addressed to J.d.W. (jdewit@mit.edu).

**Reviewer Information** *Nature* thanks D. Ehrenreich and the other anonymous reviewer(s) for their contribution to the peer review of this work.

## METHODS

**HST WFC3 observations.** We observed the transit of TRAPPIST-1c followed 12 minutes later by the transit of TRAPPIST-1b on 4 May 2016. Observations were conducted using the HST/WFC3 infrared G141 grism (1.1–1.7 μm) in round-trip scanning mode[10]. Using the round-trip scanning mode involves exposing the telescope during an initial forward slew in the cross-dispersion direction, and exposing during an equivalent slew in the reverse direction (details on the trade-offs behind round-trip scanning are below). Scans were conducted at a rate of ∼0.236 pixels per second, with a final spatial scan covering ∼26.4 pixels in the cross-dispersion direction on the detector.

We use the IMA output files from the CalWF3 pipeline, which have been calibrated using flat fields and bias subtraction. We applied two different extraction techniques which lead to the same conclusions. The first technique extracts the flux for TRAPPIST-1 from each exposure by taking the difference between successive non-destructive reads. A top-hat filter[27] is then applied around the target spectrum, measured ±18 pixels from the centre of the TRAPPIST-1 scan, and sets all external pixels to zero. Next, the images are reconstructed by adding the individual reads per exposure back together. Using the reconstructed images, we extracted the spectra with an aperture of 31 pixels around the computed centring profile for both forward and reverse scan observations. The centring profile is calculated on the basis of the pixel flux boundaries of each exposure, which was found to be fully consistent across the spectrum for both scan directions.

The second technique uses the final science image for each exposure and determines for each frame the centroid of the spectrum in a box 28 pixels by 136 pixels, which corresponds to the dimensions of the irradiated region of WFC3's detector for our present observations. It then extracts the flux for 120 apertures of sizes ranging along the dispersion direction from 24 pixels to 38 pixels (with 1-pixel increments), and along the cross-dispersion direction from 120 pixels to 176 pixels (with 8-pixel increments)—we found the SDNR to be mostly insensitive to the aperture size along the dispersion direction. The best aperture was selected via minimization of the SDNR of the white-light-curve best fit, which is minimum for an aperture of 32 pixels by 157 pixels.

Both techniques subtract the background for each frame by selecting a region well away from the target spectrum, calculating the median flux, and cleaning cosmic-ray detections with a customized procedure[28]. Our observations present three cosmic-ray detections that were not flagged by the CalWF3 pipeline. The exposure times were converted from Julian date in universal time (JDUT) to the barycentric Julian date in the barycentric dynamical time (BJDTDB) system[29]. Both extraction methods result in the same relative flux measurements from the star and SDNR (∼240 p.p.m. in the white-light curve), as the build-up of flux over successive reads is stable.

We elected to obtain our observations using the round-trip scan mode in order to increase the integration efficiency compared with the standard forward scan mode. We note that, owing to slight differences in scan length/position and to the way in which the detector is read out (that is, if the direction of the scan is in the same direction as the column readout, then the integration time will be marginally longer than if the reverse were true[10]), round-trip scan mode results in measurable differences in the total flux of the forward scan exposures compared with the reverse scan exposures. This effect has been seen for previous WFC3 observations[14,30] in round-trip mode, and has been corrected for in two main ways.

The first method involves splitting the data into two sets, one for forward scan exposures and one for reverse scan exposures, effectively halving the number of exposures per light curve, but doubling the number of light curves obtained. Each of these data sets is then analysed separately and the results combined at the end[14]. The second method uses the median of each scan direction to normalize the two light curves, which are then recombined and normalized before the light-curve analysis to obtain the transit parameters[30]. In the TRAPPIST-1 data, we measure a ∼0.1% difference in flux level between the two scans. Because of the limited phase coverage of the combined transits, to retain the most information about the combined and separate effects of each planet (the transit of TRAPPIST-1c followed by that of TRAPPIST-1b), we cannot apply the first method. However, by applying the second method we found significant remaining structure in the residuals, suggesting that the correction is only partial. Previous observations using the round-trip scan[30] show that the offset between the light curves obtained with each scan varies significantly from orbit to orbit, suggesting that correcting via a median combine across visits is not optimal. In addition, the total flux is affected asymmetrically by other instrumental systematics—for example, the detector ramp consistently yields a first measurement in the forward direction that is significantly lower than average—thus biasing the median combine. Therefore, we corrected for the flux offset induced by the round-trip scan mode on the basis of the offset in the residuals for each HST orbit individually. To do so, we estimate in our forward model the 'intermediate residuals', based on the data corrected for the transit model and the instrumental systematics. For each orbit, we estimate the mean of these residuals for each scan direction ($m_f$ and $m_r$, for the mean of the residuals of the forward-scan exposures and the reverse-scan exposures, respectively). The ratio of the fluxes measured in reverse-scan exposures to the shared baseline level is $1+m_r$; the ratio is $1+m_f$ for forward-scan exposures. We therefore correct for their offsets by dividing each set of exposures by their respective ratio.

**HST WFC3 white-light curve and spectroscopy.** We first analysed the white-light curve by summing the flux across all wavelengths. We fitted the transits of TRAPPIST-1b and TRAPPIST-1c by using the transit model of ref. 17, while correcting for instrumental systematics. We followed the standard procedure for analysing HST/WFC3 data by fixing the planets' orbital configurations—all but the orbital inclinations, which are currently poorly constrained for TRAPPIST-1's planets—to the ones reported in the discovery report[3], while determining the transit times and depths. We used priors on the band-integrated limb-darkening coefficients (LDCs) derived from the PHOENIX model intensity spectra[15], and on the planets' orbital inclinations—these parameters being potentially correlated with the transit depth estimates—to adequately account for our present state of knowledge on TRAPPIST-1. We used different analysis methods to confirm the robustness of our conclusions.

The first method uses a least-squares minimization fitting (L–M) implementation[12] to investigate a large sample of systematic models—which include corrections in time, HST orbital phase, and positional shifts in wavelength on the detector—and marginalize over all possible combinations to obtain the transit parameters. The L–M implementation fits the light curves for each systematic model and approximates the evidence-based weight of each systematic model using the Akaike information criterion[31]. It does so while keeping the LDCs fixed to the best estimates presented below, and the orbital inclinations fixed to the estimates from ref. 3. The highest weighted systematic models include linear corrections in time, as well as linear corrections in HST orbital phase or in the shift in wavelength position over the course of the visit. Therefore, using marginalization across a grid of stochastic models allows us to account for all tested combinations of systematics and to obtain robust transit depths for both planets, separately and in combination. For this data set, the evidence-based weight approximated for each of the systematic models applied to the data indicates that all of the systematic models fit equally well to the data, and that no one systematic model contributes to the majority of the corrections required to obtain the precision presented (Extended Data Fig. 1). In other words, instrumental systematics affect our observations only marginally. We carried out independent analyses of the data by using adaptive Markov chain Monte Carlo (MCMC) implementations[32,33]. For each HST light curve, the transit models[17] of TRAPPIST-1b and TRAPPIST-1c are multiplied by baseline models that account for the visit-long trend observed in WFC3 light curves, WFC3's ramp, and the 'HST breathing' effect[12]. For these analyses, priors are used for the LDCs and the orbital inclinations. We find that the visit-long trend is adequately accounted for with a linear function of time, the ramp with a single exponential in time, and the breathing with a second-order polynomial in HST's orbital phase. More-complex baseline models were tested and gave consistent results, as revealed by the marginalization study.

We calculated the transmission spectrum by fitting the transit depth of TRAPPIST-1b and TRAPPIST-1c simultaneously in each spectroscopic light curve. We divided the spectral range between 1.15 μm and 1.7 μm into 11 equal bins of $\Delta\lambda = 0.05$ μm. We applied again the two techniques described above to analyse each spectroscopic light curve, resulting in the combined and independent transmission spectra of TRAPPIST-1b and TRAPPIST-1c. An L–M implementation[12] and the adaptive MCMC implementations produced consistent results for each stage of the analysis.

**Limb-darkening coefficients.** We determined limb-darkening coefficients by fitting theoretical specific intensity spectra ($I$) downloaded from the Göttingen spectral library (http://phoenix.astro.physik.uni-goettingen.de/?page_id=73), which is described in ref. 15. The intensity spectra are provided on a wavelength grid with 1-Å cadence for 78 $\mu$ values, where $\mu$ is the cosine of the angle between an outward radial vector and the direction towards the observer at a point on the stellar surface. We integrated $I$ over one broad and 11 narrow wavelength intervals, used in our analysis of the transit light curve. We divided $I$ for each wavelength interval by $I_c$, the value of $I$ at the centre of the stellar disc (where $\mu = 1$).

Because the PHOENIX code calculates specific intensity spectra in spherical geometry, the PHOENIX $\mu$ grid extends above the stellar limb relevant to exoplanet transit calculations. When fitting limb-darkening functions, PHOENIX $\mu$ values should be scaled to yield $\mu' = 0$ at the stellar radius[34]. We define $\mu' = (\mu - \mu_0)/(1 - \mu_0)$, where $I/I_c = 0.01$ at $\mu = \mu_0$. The value of $\mu_0$ is a function of wavelength. We then fitted two commonly used functional forms for limb darkening[18]:

$$I/I_c = 1 - a(1 - \mu') - b(1 - \mu')^2$$

and

$$I/I_c = 1 - c_1(1 - (\mu')^{1/2}) - c_2(1 - \mu') - c_3(1 - (\mu')^{3/2}) - c_4(1 - \mu')^2$$

When fitting, we ignored points with $\mu' < 0.05$.

Extended Data Fig. 2 shows the limb-darkening fits for the 12 wavelength intervals in our transit light curve analysis. We calculated fits for four stellar models with effective temperatures of 2,500 K and 2,600 K and logarithmic surface gravities of 5.0 and 5.5. We then linearly interpolated the limb-darkening coefficients to an effective temperature of 2,550 K and gravity 5.22, appropriate for TRAPPIST-1 (ref. 3).

**Transmission spectrum models.** We simulated the theoretical spectra for TRAPPIST-1b and TRAPPIST-1c using the model introduced in ref. 19. We used atmospheric temperatures equal to the planets' equilibrium temperatures assuming a Bond albedo of 0.3 (these temperatures being 366 K for TRAPPIST-1b and 315 K for TRAPPIST-1c). The use of isothermal temperature profiles set at the equilibrium temperatures is conservative, as it does not account for possible additional heat sources or temperature inversion and results in a possible underevaluation of the atmospheric scale height. Our assumption regarding the temperature profiles does not affect our conclusion; variations of 50 K (that is, ~15%) in the atmospheric temperature modify the amplitude of the transmission spectra by up to ~15%, because at first order their amplitudes scale with the temperature. The planetary masses being unconstrained, we conservatively use a mass of $0.95M_\oplus$ and $0.85M_\oplus$ for TRAPPIST-1b and TRAPPIST-1c respectively—the maximum masses that would allow them to possess hydrogen/helium envelopes greater than 0.1% of their total masses given their radii[20]. We use the atmospheric compositions of the 'mini-Neptune' and 'Halley world' models introduced in ref. 35 to simulate the hydrogen-dominated and water-dominated atmospheres, respectively. We simulated the effect of optically thick cloud or haze at a given pressure level by setting to zero the transmittance of atmospheric layers with a higher pressure.

The feature at 1.4 μm arises from water absorption; the feature at 1.15 μm for the water-dominated atmosphere arises from methane absorption. We compared the transmission spectra, allowing for a vertical offset to account for our *a priori* ignorance of the optically thick radius by setting the mean of each spectrum to zero. The significance of the deviation of each transmission spectrum from the WFC3 measurements is shown in Fig. 3. Significance levels less than $3\sigma$ mean that the data are consistent with that model within the reported errors.

We rule out the presence of a cloud-free hydrogen-dominated atmosphere for either planet at the $10\sigma$ level through the combined transmission spectrum (and at a lesser $7\sigma$ level through their individual spectra). The measurements are consistent with volatile (for example, water)-rich atmospheres or hydrogen-dominated atmospheres with optically thick clouds or hazes located at larger pressures than 10 mbar.

**Code availability.** Conversion of the UT times for the photometric measurements to the BJDTBD system was carried out using the online program created by J. Eastman and distributed at http://astroutils.astronomy.ohio-state.edu/time/utc2bjd.html. We have opted not to make available the codes used for data extraction as they are an important part of the researchers' toolkits. For the same reason, we have opted not to make available all but one of the codes used for data analysis. The MCMC software used by M.G. to analyse independently the photometric data is a custom Fortran 90 code that can be obtained upon request. The custom IDL code used to determine limb-darkening coefficients can be obtained upon request.


27. Evans, T. M. *et al.* Detection of $H_2O$ and evidence for TiO/VO in an ultra-hot exoplanet atmosphere. *Astrophys. J.* **822,** L4 (2016).
28. Huitson, C. M. *et al.* An HST optical-to-near-IR transmission spectrum of the hot Jupiter WASP-19b: detection of atmospheric water and likely absence of TiO. *Mon. Not. R. Astron. Soc.* **434,** 3252–3274 (2013).
29. Eastman, J., Siverd, R. & Gaudi, B. S. Achieving better than 1 minute accuracy in the heliocentric and barycentric Julian dates. *Publ. Astron. Soc. Pacif.* **122,** 935–946 (2010).
30. Knutson, H. A. *et al.* Hubble Space Telescope near-IR transmission spectroscopy of the super-Earth HD 97658b. *Astrophys. J.* **794,** 155 (2014).
31. Gibson, N. P. Reliable inference of exoplanet light-curve parameters using deterministic and stochastic systematics models. *Mon. Not. R. Astron. Soc.* **445,** 3401–3414 (2014).
32. Gillon, M. *et al.* The TRAPPIST survey of southern transiting planets. I. Thirty eclipses of the ultra-short period planet WASP-43 b. *Astron. Astrophys.* **542,** A4 (2012).
33. de Wit, J. *et al.* Direct measure of radiative and dynamical properties of an exoplanet atmosphere. *Astrophys. J.* **820,** L33 (2016).
34. Espinoza, N. & Jordán, A. Limb darkening and exoplanets: testing stellar model atmospheres and identifying biases in transit parameters. *Mon. Not. R. Astron. Soc.* **450,** 1879–1899 (2015).
35. Benneke, B. & Seager, S. Atmospheric retrieval for super-Earths: uniquely constraining the atmospheric composition with transmission spectroscopy. *Astrophys. J.* **753,** 100 (2012).

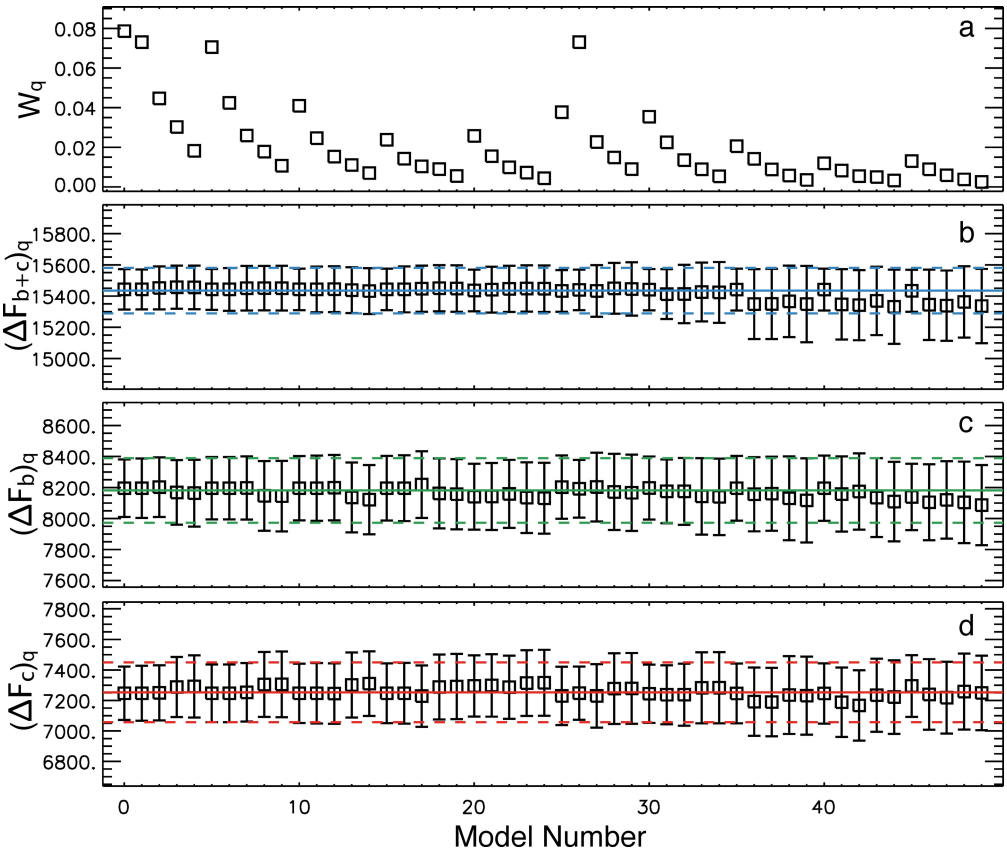


**Extended Data Figure 1 | Marginal effects of instrumental systematics on transit depth estimates. a**, Evidence-based weight, $W_q$, for each systematic model[12] applied to the white-light curve. **b**, Combined transit depth estimate ($\Delta F_{b+c}$) obtained by correcting the data, using each systematic model. **c**, **d**, Individual transit depth estimates for TRAPPIST-1b and TRAPPIST-1c, $\Delta F_b$ and $\Delta F_c$. The horizontal lines indicate the final marginalized measurements and associated uncertainties. The scale of the values here indicates that all of the systematic models fit equally well to the data.

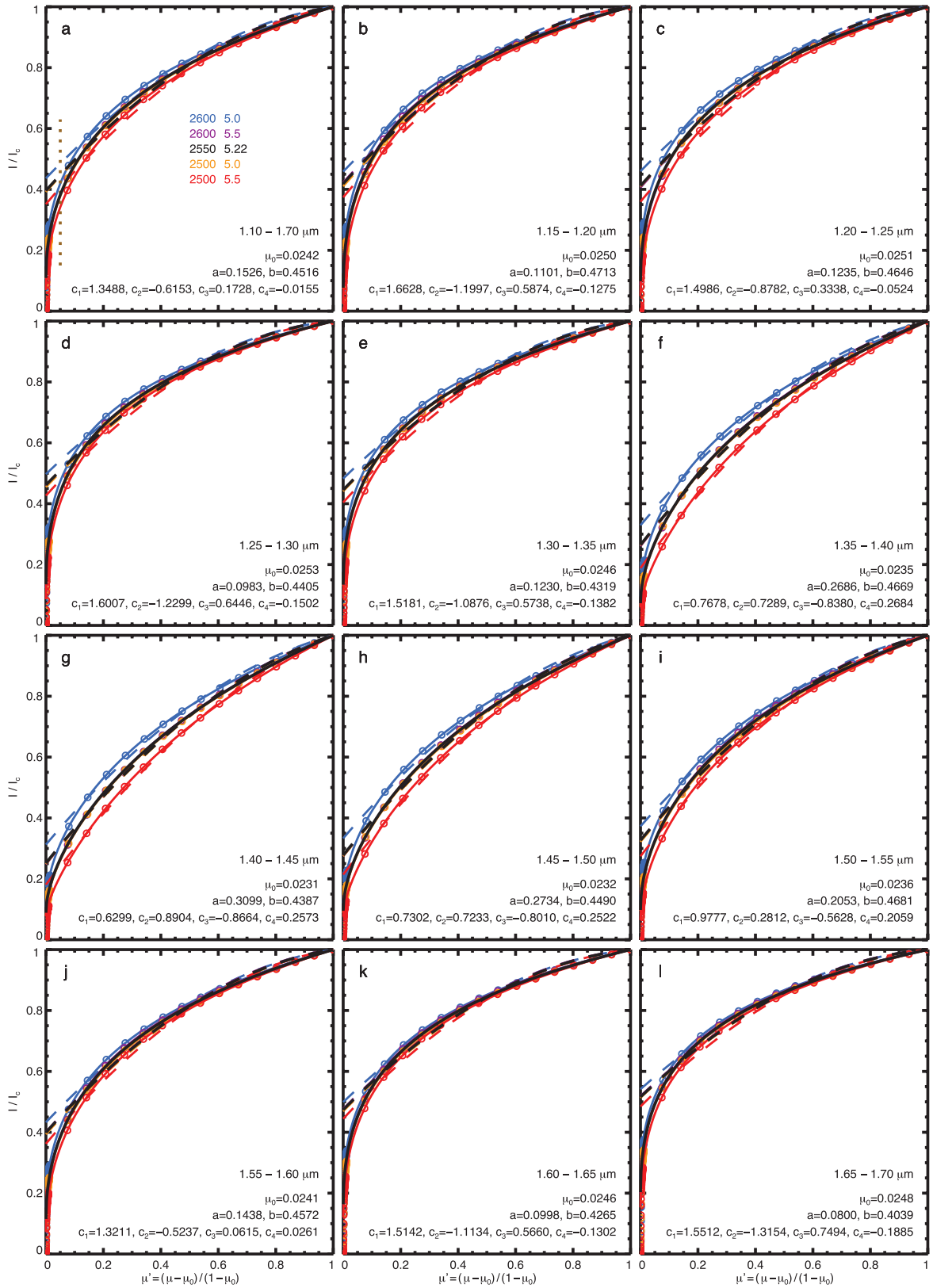


**Extended Data Figure 2 | TRAPPIST-1's limb darkening.** Stellar limb-darkening relationships for TRAPPIST-1 (black curves) and four stellar models (coloured curves) that bracket the effective temperature and surface gravity of TRAPPIST-1 (shown in coloured and black numbers in **a**; temperature is in K and surface gravity is expressed in log($g$). The circles are theoretical[15] specific intensities ($I$) relative to disc centre ($I_c$) as a function of $\mu'$ (the cosine of the angle between an outward radial vector and the direction towards the observer). We fitted $I/I_c$ averaged over the indicated wavelength intervals to determine the quadratic (dashed curves) and four-parameter (solid curves) limb-darkening coefficients. **a**, Stellar limb-darkening relationship integrated over WFC3's spectral band. **b**–**l**, Stellar limb-darkening relationship over the 11 spectral channels used here.